JTTEE5 10:461-469
© ASM International

Computational Fluid Dynamic Modeling of Gas Flow Characteristics in a High-Velocity Oxy-Fuel Thermal Spray System

S. Gu, C.N. Eastwick, K.A. Simmons, and D.G. McCartney

(Submitted 1 August 2000)

A computational fluid dynamics (CFD) model is developed to predict gas dynamic behavior in a high-velocity oxy-fuel (HVOF) thermal spray gun in which premixed oxygen and propylene are burnt in a 12 mm combustion chamber linked to a parallel-sided nozzle. The CFD analysis is applied to investigate axisymmetric, steady-state, turbulent, compressible, and chemically combusting flow both within the gun and in a free jet region between the gun and the substrate to be coated. The combustion of oxygen and propylene is modeled using a single-step, finite-rate chemistry model that also allows for dissociation of the reaction products. Results are presented to show the effect of (1) fuel-to-oxygen gas ratio and (2) total gas flow rate on the gas dynamic behavior. Along the centerline, the maximum temperature reached is insensitive to the gas ratio but depends on the total flow. However, the value attained (~2500 K) is significantly lower than the maximum temperature (~3200 K) of the annular flame in the combustion chamber. By contrast, the centerline gas velocity depends on both total flow and gas ratio, the highest axial gas velocity being attained with the higher flow and most fuel-rich mixture. The gas Mach number increases through the gun and reaches a maximum value of approximately 1.6 around 5 mm downstream from the nozzle exit. The numerical calculations also show that the residual oxygen level is principally dependent on the fuel-to-oxygen ratio and decreases by approximately fivefold as the ratio is varied from 90 to 69% of the stoichiometric requirement. The CFD model is also used to investigate the effect of changes in combustion chamber size and geometry on gas dynamics, and the results are compared with the nominal 12 mm chamber baseline calculations.

Keywords CFD, gas dynamics, HVOF, modeling

1. Introduction

High-velocity oxy-fuel (HVOF) thermal spray guns are now being widely used to produce protective coatings, typically, 200 to 800 μm thick, on the surfaces of engineering components.[1,2] Materials being sprayed include metallic alloys, cermets, ceramics, and polymers. In the HVOF process, oxygen and a fuel gas are mixed and burnt in a combustion chamber at high flow rates and pressures in order to produce a high-temperature, high-speed gas jet.[2,3] Powder particles, normally in the size range 5 to 65 μm, are injected into the jet so that they are heated as they are accelerated toward the substrate to be coated. On arrival at the substrate, particles are ideally in a softened state (they may indeed be partially or fully molten) and, on impact, form lenticular splats, which adhere well to the substrate and to one another. The HVOF gun is scanned across the substrate to build up the required coating thickness in a number of passes.

The properties of a thermally sprayed coating are strongly influenced by the microstructure of the deposit and the phases formed within it. These, in turn, will be directly determined by the process parameters, such as fuel-to-oxygen ratio, total gas flow rate, standoff distance between gun and substrate, and powder particle size range. Although there have been many parametric studies performed on the relationship between process control parameters and coating performance, such an approach does not generally provide a fundamental understanding of the complex interactions, which take place in an HVOF gun. It is in this context that numerical modeling, based on computational fluid dynamical (CFD) analysis, of gas flow and heat transfer within a HVOF thermal spray system is of importance if the process is to achieve its full potential.[3]

Several previous numerical CFD simulations have investigated gas and particle flows in HVOF thermal spray guns. Power *et al.*[4] and Smith *et al.*[5] modeled a Metco Diamond Jet gun (Sulzer Metco, Westbury, NY) using a steady-state axisymmetric analysis. In the Diamond Jet system, premixed oxygen (O_2) and propylene (C_3H_6) are injected into an air-cooled nozzle. They modeled the internal flow and external flow separately with a finite-rate chemistry model in the internal flow and equilibrium chemistry results as boundary conditions for the external flow. Oberkampf and Talpallikar[6,7] also developed a model of a similar gun geometry, again using an axisymmetric, steady-state analysis. In their work, there was full coupling between the interior and exterior flow fields, and an approximate equilibrium chemistry model was used to treat the combustion of C_3H_6.

Work by Hassan *et al.*[8] involved a three-dimensional CFD analysis of the gas dynamics in a HVOF thermal spray torch similar to the Diamond Jet Rotating Wire system (Sulzer Metco). In this system, premixed oxygen and propylene are also injected into an air-cooled nozzle, and they employed an instantaneous equilibrium chemistry combustion model. More recently, Lopez *et al.*[9] have extended this three-dimensional CFD analysis and modeled combustion by a single-step, finite-rate chemistry approach. Flow and temperature fields inside and outside the noz-

---

S. Gu, C.N. Eastwick, K.A. Simmons, and **D.G. McCartney,** School of Mechanical, Materials, Manufacturing Engineering and Management, University of Nottingham, Nottingham, NG7 2RD, United Kingdom. Contact e-mail: graham.mccartney@nottingham.ac.uk.

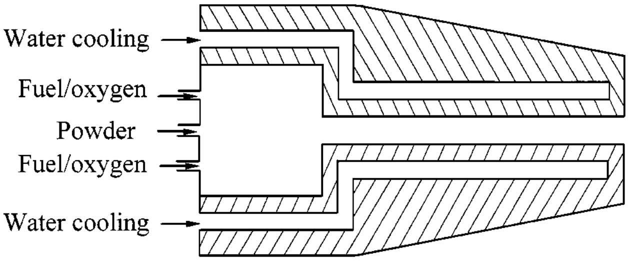

Fig. 1 Schematic representation of the HVOF gun geometry (not to scale), showing premixed fuel and oxygen entering the combustion chamber, which is connected to a parallel-sided nozzle. The dimensions of the various components are listed in Table 1

Table 1 Dimensions of the principal components of the HFOF gun shown in Fig. 1

Component	Dimension/mm
Combustion chamber (nominal 12 mm size)	14 by 23.7 (length by diameter)
Nozzle	115 by 7.7 (length by diameter)
Powder/carrier gas injector	1.1 (diameter)
Propylene/oxygen injector	0.9 (annular width)

zle were determined and particle velocities computed. The latter were found to be in reasonable agreement with laser two-focus velocimetry measurements.

Chang and Moore[10] studied the transient flow and temperature distribution in a liquid-fueled HVOF gun similar to the JP-5000 system (Praxair & Tafa Thermal Spray Products, Appleton, WI). In this gun, oxygen and kerosene are injected into the combustion chamber and gaseous products are accelerated through a converging-diverging throat and along a barrel. They assumed complete combustion of the fuel, allowed for chemical reactions of the gaseous products in the flow through the throat and barrel, but did not simulate the free jet external to the gun. A steady-state solution was found to develop in less than 2×10^{-3} s, and, in this system, Mach numbers greater than one were calculated to develop inside the barrel because of the converging-diverging design of the throat of the burner.

In the current work, a computational model was developed for an HVOF gun design similar to the Praxair HV2000 system (Praxair & Tafa Thermal Spray Products). A schematic representation of this gun is shown in Fig. 1 and relevant dimensions are given in Table 1. Oxygen and propylene are injected into the water-cooled combustion chamber, through an annular array of fine orifices, where the gases burn and the combustion products are accelerated down the parallel-sized nozzle. Powder particles are injected axially into the combustion chamber by a carrier gas flow (nitrogen or oxygen). The particle laden gas mixture then exits the nozzle at a high temperature and velocity toward the substrate to be coated, which is typically placed 200 to 300 mm from the end of the nozzle. A CFD analysis is applied to investigate the gas dynamic behavior and this paper presents the results of steady-state, axisymmetric flow calculations for turbulent, fully compressible, high-speed, chemically combusting gas flows within the gun and in the free jet region between the gun and substrate. The relative importance of the total gas flow rate and the fuel-to-oxygen gas ratio on gas temperatures, velocities, and residual oxygen levels in the gun are the principal features examined. However, the effect of combustion chamber design on the gas dynamics is also briefly investigated. A subsequent paper will present results on particle motion and heating within the gas flow fields.

2. Computational Model

2.1 Fluid Dynamics

The two-dimensional, axisymmetric, steady-state simulations are performed in the commercially available finite volume CFD code CFX 4.2,[11] which is a fully viscous Navier-Stokes solver. The basic sets of equations solved by CFX are those for the conservation of mass, momentum, and energy in a compressible, turbulent chemically reacting flow. The standard k-ϵ turbulence model is applied along with the SIMPLE pressure correction algorithm. Species transport equations are solved for each of the species in the chemical combustion reactions described in Section 2.2.

2.2 Chemical Reactions

In the present work, the propylene-plus-oxygen inlet stream (Fig. 1) is assumed to be completely mixed, and combustion of propylene is analyzed in the combustion chamber using a finite reaction rate chemistry model.[11] Classically, the end products of propylene combustion are regarded as carbon dioxide and water:

$$C_3H_6 + 4.5O_2 \rightarrow 3CO_2 + 3H_2O \qquad \text{(Eq 1)}$$

However, when temperatures in excess of 2000 K are reached, CO_2 and H_2O will dissociate into a number of different species such that the equilibrium reaction, for an oxygen-to-fuel ratio, f, becomes

$$\begin{aligned} C_3H_6 + fO_2 \rightarrow\ & n_1CO_2 + n_2CO_2 + n_3H_2O \\ & + n_4H_2 + n_5OH + n_6H + n_7O_2 + n_8O \qquad \text{(Eq 2)} \end{aligned}$$

where the n_i values represent the equilibrium number of moles of each of the products of the reaction. For a constant total pressure, the partial pressure equilibrium constants depend on temperature alone, and so, at any temperature, the n_i values can, in principle, be uniquely determined for a given value of oxygen-to-fuel ratio. Furthermore, the theoretical adiabatic flame temperature is the one, unique temperature where the net heat of combustion exactly equals the enthalpy change of the species present. The approaches for calculating equilibrium combustion reactions, taking into account dissociation, are described in detail by Hewitt[12] and Gordon and McBride,[13] and reactions such as Eq 2, determined for appropriate temperatures and pressures, are employed in the present combustion analysis. However, as well as specifying a reaction and its associated enthalpy release, it is necessary to simulate heat evolution using a finite-rate model. Hassan *et al.*[8] have previously demonstrated that a global, one-step chemistry rate model adequately represents the combustion of propylene, and this approach is also adopted in the present study. The rate expression, k, of the one-step, global

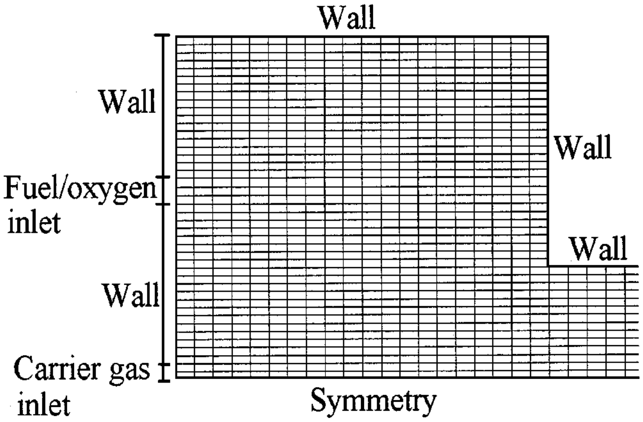

Fig. 2 Computational grid within the 14 mm long combustion chamber (nominal size 12 mm) and entrance to the parallel-sided nozzle. The centerline symmetry axis is shown

Table 2 Inlet gas flow rates and temperatures for baseline calculations (refer to Appendix I for conversion factors)

Gas	Flow rate/SCFH	Temperature/K
C_3H_6 (fuel)	150	288
O_2	555	288
N_2 (carrier)	35	288

reaction is expressed as

$$k = AT^n \exp(-E_a/RT)\,[C_3H_6]^a\,[O_2]^b \qquad \text{(Eq 3)}$$

where T is the gas temperature in Kelvin; E_a is the activation energy; $[C_3H_6]$ and $[O_2]$ are fuel and oxygen concentrations, respectively; R is the universal gas constant; and A, n, a, and b are constants given, along with E_a, for the combustion of propylene by Westbrook and Dryer.[14]

2.3 Computational Domain, Grid Geometry, and Boundary Conditions

For the gun geometry shown in Fig. 1, the flow is assumed axisymmetric and the computational domain covers the combustion chamber, the parallel-sided nozzle, and an external region to allow the development of the free jet. The external domain extends 15 nozzle exit diameters from the symmetry line in the radial direction and 20 nozzle exit diameters from the nozzle exit in the axial direction (from Table 1, the nozzle exit diameter is 7.7 mm). Inside the combustion chamber, the computational grid comprises 20 axial and 50 radial cells, as illustrated in Fig. 2, which are uniformly spaced in both directions. In the nozzle, the grid is composed of 14 radial by 250 axial cells, which are clustered toward the nozzle exit in the axial direction and uniformly spaced radially. The computational grid in the external domain is shown in Fig. 3. There are 7300 external cells, which are arranged nonuniformly in order to better capture the compressible flow characteristics at the nozzle exit and in the region of rapid jet decay, while allowing for large cells where flow magnitudes and directions are changing only relatively slowly. In the present analysis, the fuel-oxygen inlet stream is modeled as an annular ring that has the same total area as the equally spaced inlet holes (which exist in practice) and is centered at the same radial location as the holes. Carrier gas flows in through the powder inlet orifice, but, in the present analysis, a solid particle flow was not included.

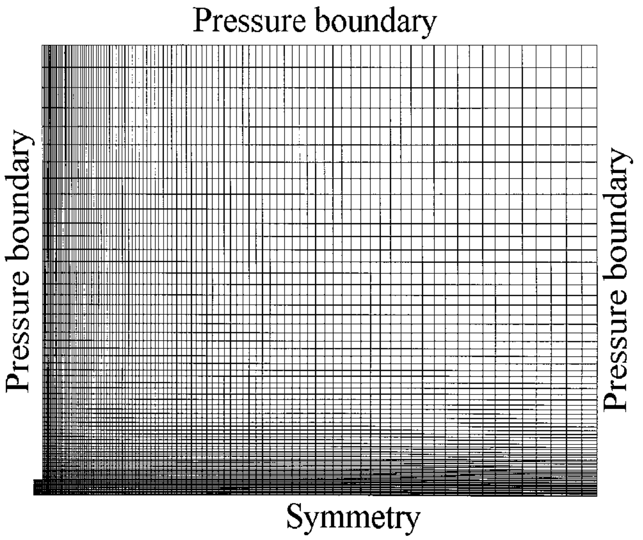

Fig. 3 Exterior computational grid showing symmetry axis, pressure boundaries, and outflow boundary (right-hand side). The nozzle exit is at the bottom left-hand corner where the cell spacing is not resolved

Table 2 lists the inlet gas flow rates and temperatures that were employed to investigate the basic flow characteristics, as reported in Section 3.1. Values are given in standard cubic feet per hour (SCFH), as this is the practical unit used on many control consoles for this gun system. However, Appendix I provides conversion factors to other systems of units. The nozzle is assumed to exhaust to air, which is at an ambient temperature and pressure of 298 K and 1.01×10^5 Pa, respectively. In the exterior grid (Fig. 3), the pressure boundaries have temperature and pressure fixed as above, while the outflow boundary is specified as one with a zero pressure gradient in the radial direction. In the interior grid, all boundary surfaces are specified to be no-slip, fixed-temperature walls. On the basis that the combustion chamber and nozzle walls are water-cooled copper, their temperature are fixed at 373 K. The wall temperature between the inlets was set to 1000 K, as this wall is not water cooled. A total of 13,704 cells are used in the baseline calculations described in Section 3.1.

3. Steady-State Flow Fields

3.1 Baseline Calculations

The results presented in this section are for the gun geometry and grids shown in Fig. 1 to 3 with the gas flow rates as listed in Table 2. The fuel-to-oxygen ratio for this case is 0.27, which means the mixture is fuel rich compared with the stoichiometric value of 0.22 obtained from Eq 1. The oxygen level is ~82% of the stoichiometric requirement at this flow rate ratio. The gas temperature contours calculated in the combustion chamber are shown in Fig. 4. The fuel-plus-oxygen stream creates a cold jet

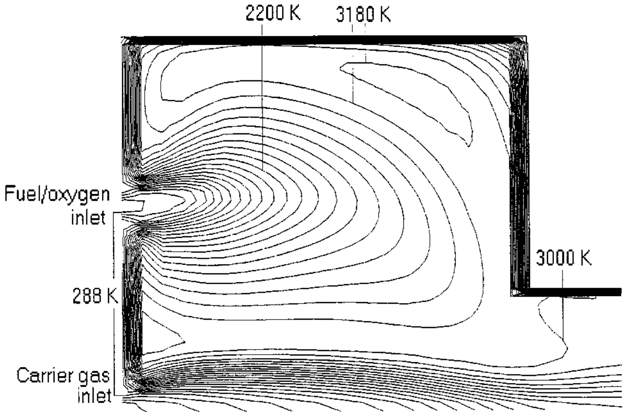

Fig. 4 Gas temperature contours in the combustion chamber for the flow conditions of Table 2

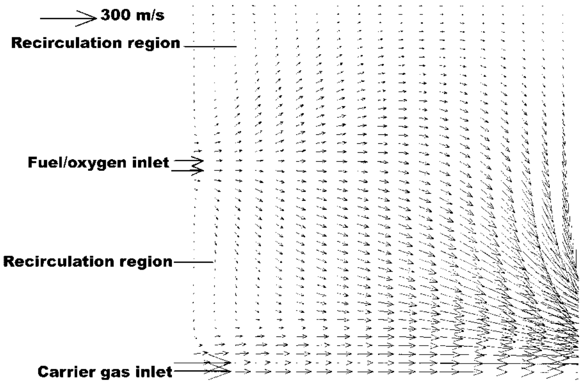

Fig. 5 Velocity vectors within the combustion chamber for flow conditions of Table 2

around which combustion develops. The orientation of the contours indicates that the flame twists slightly away from the wall toward the axis of the gun. The maximum temperature in the chamber is ~3180 K, with the hottest zones being located in the top right-hand corner and in a small region between the fuel/oxygen inlet and the carrier gas stream on the symmetry axis.

Figure 5 shows the flow pattern in the combustion chamber with a velocity vector plot. The premixed O_2 and C_3H_6 enter with a relatively low velocity (~150 ms^{-1}), although the carrier gas flow velocity at the inlet is approximately double this value because of the small cross-sectional area of the injector. The combusted gas around the flame accelerates toward the nozzle entrance, while the carrier gas stream decelerates at first before accelerating toward the nozzle entrance. The carrier gas stream deviates little from its axial flow pattern, but two small recirculation regions do appear to develop, as indicated in Fig. 5. Although powder particles are not considered in the present analysis, the gas flow pattern in the combustion chamber indicates that most of the powder would be expected to flow axially through the combustion chamber. It is clear, though, from Fig. 4 that the carrier gas effectively blankets the powder in a cooler shroud and that the powder will not come into contact with the hottest gas in the combustion chamber, *i.e.,* it will never experience the maximum flame temperature. Figure 6 shows gas Mach number contours at the exit from the nozzle, which is located at the zero of the scale in Fig. 6. Two maxima in Mach number are visible in the core structure of the jet, which emerges as an underexpanded flow with Ma ~ 1 at the exit from the parallel-sided nozzle. In practice, the jet expands to match the ambient air pressure through a series of expansion and compression waves giving rise to visible shock diamonds. This type of behavior is indeed reproduced in the CFD analysis and results in the Mach number contour structure seen in Fig. 6. The peak Mach number value of 1.62 occurs approximately 6 mm downstream from the exit plane, and the Mach number declines to a value of one approximately 60 mm downstream, as the free jet mixes with and entrains the surrounding air. Thus, the supersonic region terminates at this position, but the flow simulation also encompasses a subsonic region, since the outflow boundary is 154 mm from the nozzle exit, *i.e.,* a further 94 mm downstream from where the Mach number declines to one. An examination of the velocity vector field around the nozzle exit confirms the existence of considerable entrainment of cold air into the high-speed jet, a well-established phenomenon.[15] The peak axial velocity and temperature of the jet are around 1750 ms^{-1} and 2750 K, respectively, but axial variations in these variables will be discussed more fully in the following section.

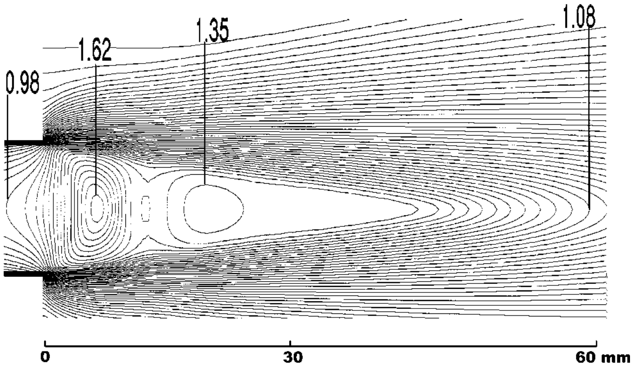

Fig. 6 Gas jet Mach number contours at the exit from the nozzle, which is located at $x = 0$ mm on the scale. Two maxima in Mach number are visible in the jet structure

3.2 Effects of Gas Flow Rate and Fuel-to-Oxygen Ratio

In this HVOF gun system, key process variables are combustion chamber length, total gas flow rate, and oxygen-to-fuel gas ratio. The results presented in this section relate once again to the gun geometry of Fig. 1 in which the combustion chamber length is 14 mm. (This was measured as the actual size of the manufacturer's nominal 12 mm length component.) The effect of varying the gas flow rate parameters will now be examined.

Two different total gas flow rates were considered, namely, 705 and 590 SCFH, and, at each of these flows, three fuel-to-oxygen ratios, namely, 0.248, 0.270, and 0.322, were investigated. The fuel flows and ratios correspond to values typical of those employed to spray materials similar to Inconel 625.[16] The above ratios are equivalent to percentage stoichiometric oxygen requirements of 90, 82, and 69%, respectively, according to Eq

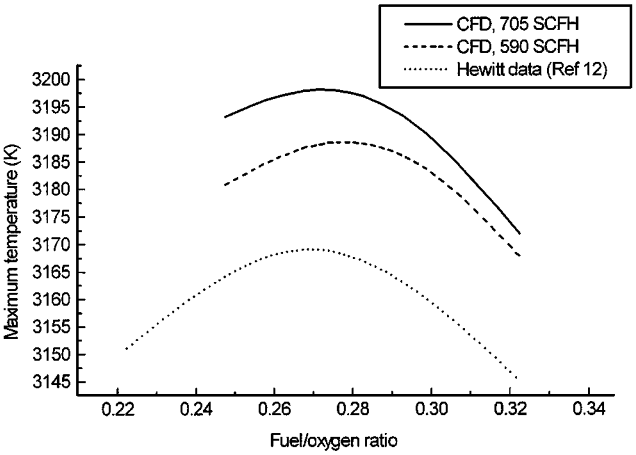

Fig. 7 Variation of maximum combustion temperature with fuel-to-oxygen ratio for CFD simulations at 705 and 590 SCFH. Also shown is the variation in adiabatic flame temperature at 1 atmosphere total pressure from Hewitt[12]

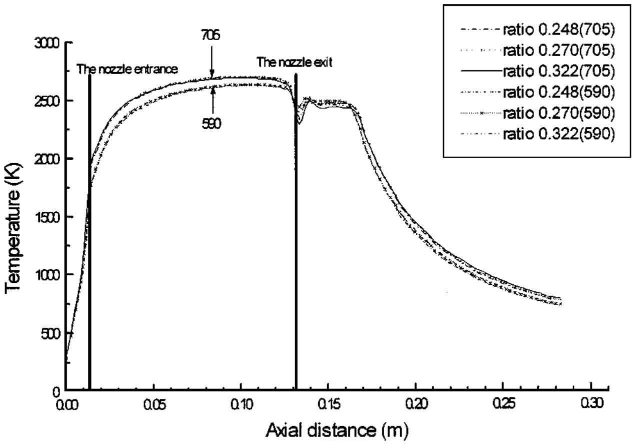

Fig. 8 Variation of gas temperature with distance along the centerline (symmetry axis) of the computational domain for gas ratios shown at flow rates of 590 and 705 SCFH

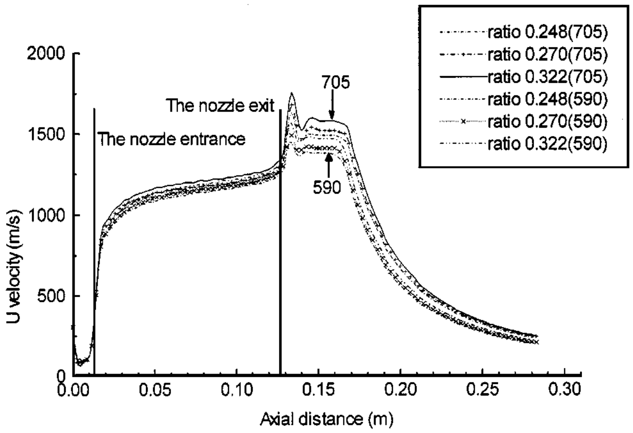

Fig. 9 Variation of axial gas velocity with distance along the centerline (symmetry axis) of the computational domain for gas ratios shown at flow rates of 590 and 705 SCFH

1\. The overall internal and external gas flow characteristics are broadly similar to those described in the previous section for the range of input flow rates and gas ratios examined. One of the significant features, however, is that the maximum temperature reached within the combustion chamber is found to vary with gas ratio, as shown in Fig. 7. There is also found to be a dependence on total gas flow with the higher flow rate, as expected, giving a marginally higher maximum combustion temperature.

The results obtained from the CFD model are compared in Fig. 7, with the adiabatic flame temperature for propylene at one atmosphere pressure calculated by Hewitt.[12] The trends in adiabatic flame temperature and CFD combustion temperature with gas ratio are seen to be similar. Although the CFD analysis included heat loss through the walls of the gun, combustion occurs at ~2 to 3 times atmospheric pressure, and it is this which presumably allows local temperatures greater than the one atmosphere adiabatic flame temperature[12] to be reached.

In considering differences among simulations, for the range of gas flows and ratios examined, results will be plotted as centerline flow field variable versus axial distance. This form of presentation is particularly relevant to developing a semi-quantitative understanding of how powder particles will be affected by different process variables, since it has already been demonstrated that the carrier gas flow remains closely aligned with the symmetry axis.

Centerline gas temperatures are plotted versus axial distance in Fig. 8. It is apparent that the gas ratio has a negligible effect on the gas temperature profile within the nozzle but that the higher total flow rate gives a higher centerline temperature. The general trend is for the gas temperature to increase sharply within the combustion chamber and to reach a plateau within the barrel before decaying in the external free jet. The temperature minimum close to the nozzle exit corresponds to the Mach number maximum in Fig. 6 and is a characteristic feature of expansion-compression waves in an underexpanded jet. The core length of the jet is ~50 mm and the temperature decays rapidly as cold air is entrained. Outside the gun, the temperature is only marginally affected by the gas flow rate. It is interesting to note that the maximum centerline temperature is around 2700 K, *i.e.*, well below the calculated adiabatic flame temperature of propylene.

Figure 9 shows the centerline axial gas velocities plotted against axial distance. The overall trend is that the velocity increases sharply as it converges into the nozzle but increases only marginally within the parallel-sided region. As it expands out of the nozzle, it develops maxima and minima as a result of compression waves just outside the nozzle and then undergoes a slow decay as air, which is entrained, reaches the centerline. The effect on velocity of changing gas flow conditions is more complicated than for the temperature field in that total flow rate and gas ratio both affect the velocity profile. A maximum velocity is achieved at the higher total flow (705 SCFH) and the highest fuel-to-oxygen ratio (0.322). Conversely, the lower flow (590 SCFH) and most oxygen-rich ratio (0.248) give the lowest velocity. Also, the three profiles for a 705 SCFH flow rate lie above those for the 590 SCFH total flow rate.

Figure 10 shows the variation of centerline gas pressure with axial distance and this demonstrates the high pressure that de-

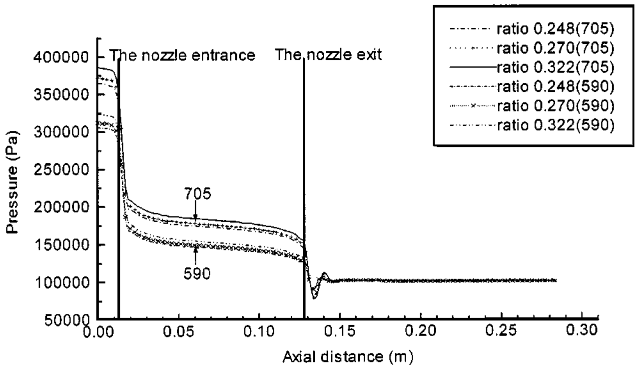

Fig. 10 Variation of gas pressure with distance along the centerline (symmetry axis) of the computational domain for gas ratios shown at flow rates of 590 and 705 SCFH

velops in the combustion chamber (~2 to 3 atmospheres relative to the surroundings). It is for this reason that this gun system requires the use of a pressurized powder feeder to supply the feedstock material being sprayed. It also shows that, at the nozzle exit, the gas is ~5×10^4 Pa above the ambient pressure and so is underexpanded. The higher total flow rate generates significantly higher gas pressures as would be expected, whereas the effect of gas ratio is rather limited.

In Fig. 11, the centerline oxygen fraction in the combustion products is plotted versus axial distance. In this case, the figure displays the variation in oxygen level from the carrier gas entrance to the nozzle exit plane. Residual oxygen arises from the fact that Eq 2 is being used to model the combustion reaction in the CFD analysis. This equation allows for dissociation of combustion products unlike Eq 1. It is for this reason that residual oxygen is present even in the fuel-rich mixtures considered here (69, 82, and 90% of stoichiometric oxygen requirements). The general trend for all flow conditions is that the oxygen level along the centerline increases as the nitrogen carrier gas stream mixes with the combustion products from the fuel/oxygen stream. The oxygen level then reaches a plateau value with the nozzle as equilibrium gas compositions are effectively reached. It is important to note that the fuel-to-oxygen ratio has a profound effect on the centerline oxygen levels. When the fuel-to-oxygen ratio is 0.32, the oxygen level is ~1/5 that when the ratio is 0.248. Conversely, the total flow rate has a rather small effect on the residual oxygen level, particularly at the lower ratio. It is thus very clear that a high fuel-to-oxygen ratio is essential to minimize oxidation or degradation reactions when oxygen-sensitive powders are being sprayed.

In summary, these steady-state flow field calculations provide significant pointers to the likely effect of process parameter changes on powder particle heating and oxidation. First, an increase in total gas flow rate at a fixed gas ratio will cause powder particles to travel at higher speeds and experience higher gas temperatures, but the effect on particle temperatures is likely to be small, since higher gas temperatures will be offset by shorter particle residence times. Second, an increase in fuel-to-oxygen gas ratio at a fixed total flow will marginally increase gas velocity with little effect on gas temperature and, hence, have very little effect on particle acceleration or heating. However, it will have a large effect on oxygen content of the gas and could thus dramatically decrease the oxidation of materials such as Ni-based alloys or WC-Co cermets. Indeed, the very significant effect of gas ratio on the oxide content of Inconel 625 coatings, sprayed using an HVOF system and conditions similar to those modeled here, has been previously reported.[16]

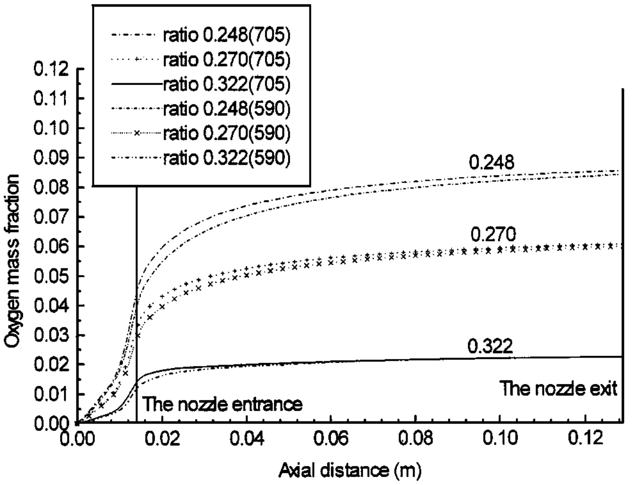

Fig. 11 Variation of oxygen content with distance along the centerline within the combustion chamber and the nozzle

4. Steady-State Flow Fields—Effect of Combustion Chamber Design

The effect of combustion chamber size and geometry is examined in this section. Specifically, combustion chambers of nominal lengths 22 and 3 mm, respectively, are considered. The objective is to understand how the chamber design affects the flow dynamics in order to provide insight into the optimum combustion chamber selection for the spraying of specific powder types. It is generally believed that a 22 mm chamber should be selected for higher melting point materials and a 3 mm one used for materials of lower melting points. Thus, in order to make appropriate comparisons, the lower and upper total gas flow rates of 590 and 705 SCFH employed in the analysis of Section 3 are used as the respective flow rates for the 3 and 22 mm chambers. The fuel-to-oxygen ratio is fixed at 0.27, *i.e.,* 82% of the stoichiometric oxygen requirement in both cases. The computational grid within the 22 mm combustion chamber is shown in Fig. 12(a). The gun dimensions are identical to those given in Table 1, except that the combustion chamber length is increased from 14 to 22 mm and the nozzle length decreased to 107 mm. The grid comprises 35 axial and 43 radial cells in the chamber, 250 axial and 14 radial cells in the nozzle, and 128 axial by 73 radial cells in the external domain. The geometry of the 3 mm combustion chamber is significantly different and the grid for this is shown in Fig. 12(b). There is a 3 mm parallel-sided entrance leading to a 27 mm long conical section, which then connects to the 100 mm long nozzle. There is a total of 2537 cells in the chamber, 11,180 in the nozzle, and 9636 in the external domain.

Results obtained on temperature and velocity fields within the 22 mm chamber are broadly similar to those depicted in Fig.

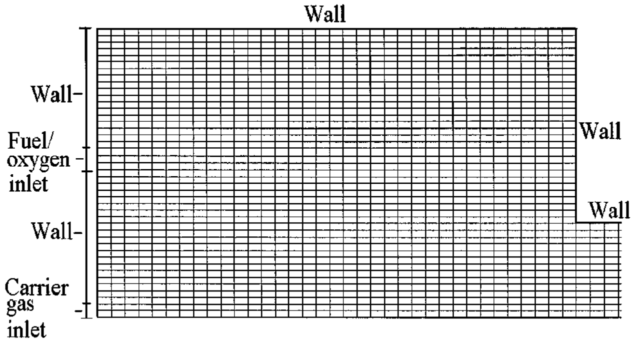

Fig. 12 Computational grid within the (**a**) 22 mm combustion chamber and (**b**) 3 mm combustion chamber

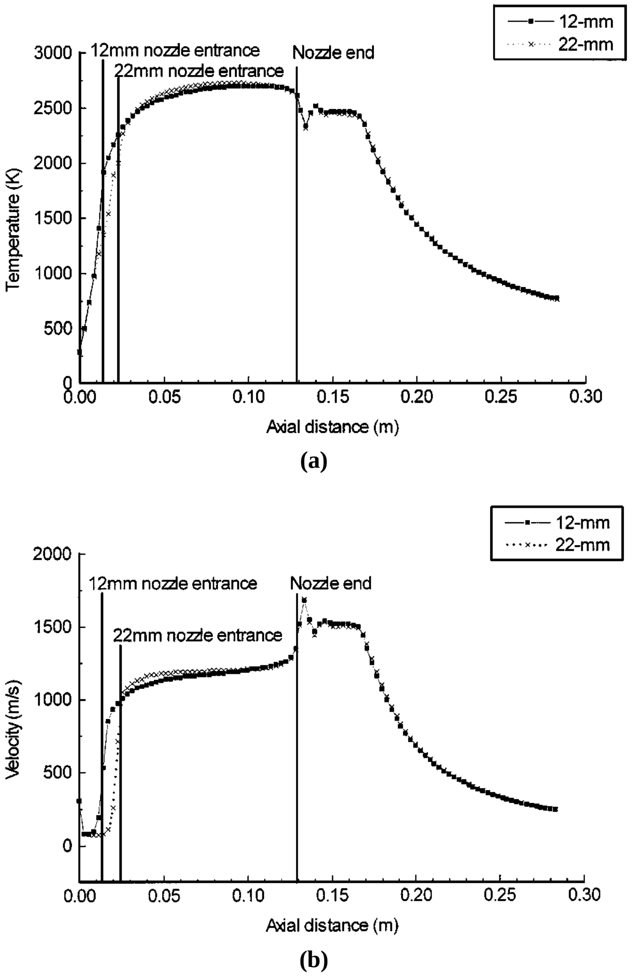

Fig. 13 Variation of (**a**) gas temperature and (**b**) axial gas velocity with distance along the centerline for the 12 and 22 mm combustion chambers with identical gas flow parameters (705 SCFH and 0.27 gas ratio)

4 and 5 for the baseline calculation with a nominal 12 mm chamber. The longer chamber allows the flame to extend more fully into a conical shape with a maximum temperature ~15 K higher. Two small recirculation zones are also found, located in similar positions to those seen in Fig. 5. Comparisons of centerline gas temperature and axial velocity variations are given in Fig. 13(a) and (b). Outside the nozzle, in the free jet region, the temperature and velocity profiles are almost identical for the two chamber sizes. The main differences in gas dynamics are seen to occur around the region where the combustion chamber joins the small diameter nozzle. In the 22 mm chamber, the rise in gas temperature as the flow converges into the nozzle is marginally delayed. However, more significantly, the gas velocity remains low for a further 8 mm in the 22 mm design, as seen in Fig. 13(b), and so this would greatly increase the residence time in the combustion chamber of powder particles being sprayed. One might anticipate, therefore, that the net effect of spraying with the 22 mm chamber (at the same gas parameters) would be to increase particle heating, with only a marginal affect on particle velocity, when compared to the behavior of a 12 mm chamber. This is generally confirmed by practical experience with this type of gun system.

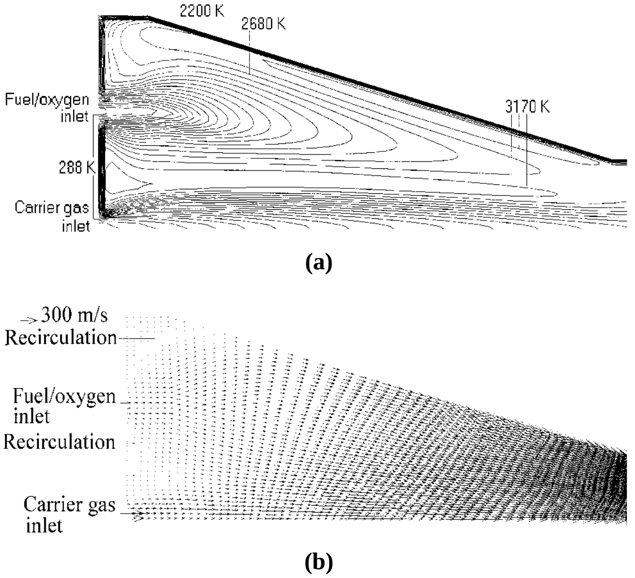

Fig. 14 (**a**) Gas temperature contours and (**b**) velocity vector plot in the 3 mm combustion chamber for the flow conditions of 590 SCFH and 0.27 gas ratio

The computations for the 3 mm chamber were run at 590 SCFH and a ratio of 0.27, and Fig. 14 shows the gas temperature contours and flow velocity field obtained. It is clear that the conical shape of the chamber has a marked effect on both temperature and flow field development. The flame twists much more noticeably toward the centerline and the hottest zone lies between the incoming, premixed O_2/C_3H_6 and N_2 (carrier gas) streams. In Fig. 14(b), the vector plot demonstrates that the flow converges much more gradually toward the nozzle entrance as compared with the abrupt change in direction seen in Fig. 5. This behavior is, qualitatively, to be expected from the conical chamber design. Comparisons of the centerline gas temperature and axial velocity variations are plotted in Fig. 15(a) and (b), respectively, for the 3 and 12 mm chamber simulations with identical gas flow conditions. The most notable difference is in the velocity variations, where the conical chamber design gives approximately the same gas velocity at the nozzle exit, but the increase in gas velocity at the nozzle entrance is much less steep.

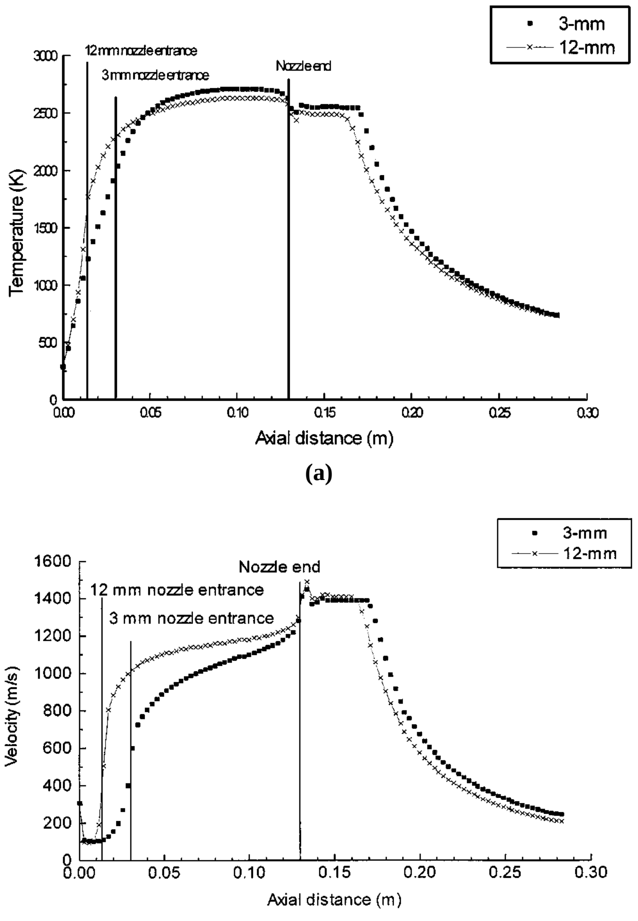

(a)

(b)

Fig. 15 Variation of (**a**) gas temperature and (**b**) axial gas velocity with distance along the centerline for the 12 and 3 mm combustion chambers with identical gas flow parameters (590 SCFH and 0.27 gas ratio)

Differences in temperature variation within the gun can also be identified with the centerline gas temperature reaching a higher value in the conical design, presumably due to the increased convergent flow induced in the combustion chamber. Outside the nozzle, in the free jet region, the decays in temperature and velocity with distance are similar for the two designs, as expected.

On the basis of these gas dynamic computations, qualitative interpretations of differences in particle heating in these two chamber designs can be drawn. Assuming the majority of powder particles travel close to the centerline, they will accelerate much less in the 3 mm chamber design, as seen from Fig. 15(b). Consequently, their dwell time will increase and they will heat up more, even though the temperature profile is only slightly different. Overall, with a 3 mm chamber, particles will probably emerge from the nozzle hotter, but traveling at a lower speed (due to the lower initial acceleration), than with a 12 mm chamber. Such behavior would increase the tendency to oxidise metallic and cermet powders. Such behavior was indeed observed by Edris *et al.*,[16] who sprayed Inconel 625 powder in a gun of similar design with different combustion chamber sizes using a very similar range of gas conditions to those modeled here. They measured coating oxygen contents by a calibrated x-ray diffraction method and their principal results are summarized in Table 3. It is apparent that greater oxide formation was found in coatings sprayed, under identical gas flow conditions, with the 3 mm combustion chamber than when the 12 mm chamber was employed. Furthermore, a change in the chamber increased the oxide content more significantly than a reduction in fuel-to-oxygen ratio. Therefore, these experimental observations support the CFD analysis in terms of the important roles of gas ratio and combustion chamber size in spraying relatively low melting point metallic alloys, which are susceptible to oxidation.

Table 3 Data from Edris *et al.*[16] relating chromium oxide contents in Inconel 625 coatings to parameter settings on a HV2000 -type of HVOF gun

Chamber size/mm	Fuel-to-oxygen gas ratio	Total flow/ SCFH	Measured wt.% Cr_2O_3
12	0.33	605	8
12	0.24	605	13
3	0.33	605	14

However, to fully quantify powder particle motion and heating in the system, a particle tracking model has to be coupled to the CFD gas dynamic analysis. Such calculations are currently being undertaken to analyze the behavior of metallic and cermet powders during spraying and the results will form the basis of a subsequent publication.

5. Conclusions

A comprehensive CFD model, using CFX, has been developed to investigate the gas dynamic behavior in an HV2000-type HVOF thermal spray gun using the fuel gas propylene premixed with oxygen. The model includes combustion *via* a chemical kinetic model and also allows for dissociation of the combustion products. The model was used to investigate the effects of two different total gas flow rates and three levels of fuel-to-oxygen gas ratio on gas temperature, composition, and flow fields. The following conclusions have been obtained.

- Inside the gun, premixed oxygen and propylene burn in the combustion chamber and the hot gas is accelerated along the parallel-sided nozzle. Although the maximum gas temperature reaches 3180 K close to the annular flame front, the centerline temperature only reaches a value of ~2500 K. The gas velocity at the end of the nozzle is ~1250 ms^{-1} with a Mach number of one. In the free jet region, the calculations predict the existence of shock diamonds as observed in practice. The peak Mach number of ~1.6 occurs about one exit diameter downstream from the nozzle exit. Air is entrained into the free jet such that the core is calculated to be approximately 7 exit diameters in length.
- Gas dynamic behavior along the centerline of the gun depends on both total gas flow rate and fuel-to-oxygen gas ratio. The numerical simulations show that the gas temperature variation depends principally on total gas flow rate and is virtually independent of gas ratio, the higher flow rate giving the higher temperature. In contrast, the axial gas velocity depends on both flow rate and ratio; the highest velocity is achieved at the higher flow rate and most fuel-rich ratio.

- Within the gun, the residual oxygen fraction along the centerline is calculated to be strongly dependent on gas ratio, and it decreases by approximately fivefold as the ratio is varied from 90 to 69% of the stoichiometric oxygen requirement. However, the influence of total flow rate on residual oxygen fraction is small.
- For this particular gun system, combustion chamber size and geometry have a significant effect on gas dynamic behavior, as is clearly revealed by comparative centerline temperature and velocity plots using the 12 mm combustion chamber as a baseline. The numerical simulations suggest that the 22 mm chamber increases the potential for particle heating, while the conical design of the 3 mm chamber has a complex effect on overall flow characteristics

Acknowledgments

The authors are extremely grateful to BOC Gases (Guilford, Surrey, United Kingdom) for financial support of this research through the award of a research studentship to SG. We also acknowledge the contributions of Gareth Arnold and Mark Cole, BOC Gases, and Geoff Creffield, formerly with BOC Gases, in interpreting computational and experimental aspects of the work.

Appendix I

Gas flow rate conversions

	Flow rate in							
Gas	**SCFH**		**l min^{-1}**		**m^3 s^{-1}**		**kg s^{-1}**	
Propylene	150	125	71	59	1.17×10^{-3}	1.00×10^{-3}	2.26×10^{-3}	1.90×10^{-3}
Oxygen	555	465	262	220	4.33×10^{-3}	3.63×10^{-3}	6.24×10^{-3}	5.22×10^{-3}
Nitrogen	35		16.5		0.27×10^{-3}		0.344×10^{-3}	

References

1. D.W. Parker and G. L. Kutner: *Adv. Mater. Processing,* 1994, vol. 7, pp. 31-35.
2. R.W. Smith and R. Knight: *J. Met.,* 1995, vol. 47, pp. 32-39.
3. V.V. Sobolev and J.M. Guilemany: *Int. Mater. Rev.,* 1996, vol. 41 (1), pp. 13-31.
4. G.D. Power, E.B. Smith, T.J. Barber, and L.M. Chiapetta: “Analysis of a Combustion (HVOF) Spray Deposition Gun,” UTRC Report No. 91-8, UTRC, East Hartford, CT, Mar. 1991.
5. E.B. Smith, G.D. Power, T.J. Barber, and L.M. Chiapetta: in *Application of Computational Fluid Dynamics to the HVOF Thermal Spray Gun, Thermal Spray: International Advances in Coatings Technology,* C.C. Berndt, ed., ASM International, Materials Park, OH, 1992, pp. 805-10.
6. W.L. Oberkampf and M. Talpallikar: *J. Thermal Spray Technol.,* 1996, vol. 5 (1), pp. 53-61.
7. W.L. Oberkampf and M. Talpallikar: *J. Thermal Spray Technol.,* 1996, vol. 5 (1), pp. 62-68.
8. B. Hassan, W.L. Oberkampf, R.A. Neiser, and T.J Roemer: in *Computational Fluid Dynamic Analysis of a High Velocity Oxygen-fuel (HVOF) Thermal Spray Torch, Thermal Spray Science and Technology,* C.C. Berndt and S. Sampath, eds., ASM International, Materials Park, OH, 1995, pp. 193-98.
9. A.R. Lopez, B. Hassan, W.L. Oberkampf, R.A. Neiser, and T.J Roemer: *J. Thermal Spray Technol.,* 1998, vol. 7 (3), pp. 374-82.
10. C.H. Chang and R.L. Moore: *J. Thermal Spray Technol.,* 1995, vol. 4 (4), pp. 358-66.
11. *CFX User’s Manual*, CFX International, AEA Technology plc, Harwell, Oxon, United Kingdom.
12. A.D. Hewitt: *Welding and Metal Fabrication,* Sept. 1972, pp. 382-89.
13. S. Gordon and B.J. McBride: “Computer Program for Calculation of Complex Chemical Equilibrium Compositions and Applications,” NASA Reference Publication No. 1311, Lewis Research Center, Cleveland, OH, Oct. 1994.
14. C.K. Westbrook and F.L. Dryer: *Combustion Sci. Technol.,* 1981, vol. 27, pp. 31-43.
15. P.O. Witze: *AIAA J.,* 1974, vol. 12, pp. 417-18.
16. H. Edris, D.G. McCartney, and A.J. Sturgeon: *J. Mater. Sci.,* 1997, vol. 32, pp. 863-72.